




# Evaluation of apoptosis in human breast cancer cell (MDA-MB-231) induced by ZnO nanoparticles synthesized using *Piper betle* leaf extract as bio-fuel

Shobha Nagarajaiah<sup>1,2,3</sup> · N. Nanda<sup>3,4</sup> · Praveen Manjappa<sup>5</sup> · Bhangi Mutta Nagabhushana<sup>6</sup> · Manoj Gadewar<sup>7</sup> · Srilatha Rao<sup>8</sup> · Prashanth Gopala Krishna<sup>9</sup> 

Received: 20 February 2023 / Accepted: 19 May 2023 / Published online: 2 June 2023  
© The Author(s), under exclusive licence to Springer-Verlag GmbH, DE part of Springer Nature 2023

## Abstract

In this investigation, zinc oxide nanoparticles (ZnO NPs) were produced by solution combustion-assisted technique utilising aqueous leaf extract of *Piper betle* (betel leaf) (PB). Phase formation and the particle size of ZnO-PB-NPs were ascertained by using X-ray diffraction. It was observed that the ZnO-PB-NPs crystallize in the hexagonal phase with an average crystallite size of 24 nm. The morphology, shape, and size of the NPs were studied by Scanning Electron Microscope and Transmission Electron Microscope (TEM). The elemental composition was analysed using energy-dispersive advanced X-ray spectroscopy. Further, Fourier-Transform Infrared (FTIR) spectroscopy confirmed the formation of ZnO bonding. Anticancer activity of ZnO-PB-NPs was evaluated in the MDA-MB-231, human breast cancer cells by MTT [3-(4, 5-dimethylthiazol-2-yl)-2, 5-diphenyl tetrazolium bromide] assay. The study findings demonstrated that the ZnO-PB-NPs were able to induce significant cytotoxicity in human breast cancer cells in a dose-dependent manner. ZnO-PB-NPs treatment impaired the Clonogenic potential cells of breast cancer. Additionally, the biocompatibility with blood components of ZnO-PB-NPs was evaluated by blood hemolysis assay. It was observed that, ZnO NPs inhibited breast cancer cell growth and increased the induction of early apoptosis cell population.

**Keywords** ZnO nanoparticles · *Piper betle* · Solution combustion · Anticancer activity · Antioxidant · Clonogenic assay · Apoptosis · Biocompatibility

✉ Shobha Nagarajaiah  
shobhamaha@gmail.com

✉ Prashanth Gopala Krishna  
prashaanthgk@gmail.com; prashanth\_chem@sirmvit.edu

<sup>1</sup> Department of Chemistry, Maharani's College for Women, Maharani Cluster University, Bengaluru, Karnataka 560001, India

<sup>2</sup> Department of Studies and Research in Chemistry, Tumkur University, Tumkur, Karnataka 572103, India

<sup>3</sup> Department of Chemistry, B.M.S. College of Engineering, Bengaluru, Karnataka 560019, India

<sup>4</sup> Department of Chemistry, BMS College for Women, Bengaluru, Karnataka 560004, India

<sup>5</sup> Center for Advanced Materials Technology (CAMT), M.S. Ramaiah Institute of Technology, Bengaluru, Karnataka 560054, India

<sup>6</sup> Department of Chemistry, Ramaiah Institute of Technology, Bengaluru, Karnataka 560054, India

<sup>7</sup> Department of Pharmacology, School of Medical and Allied Sciences, KR Mangalam University, Gurgaon, Haryana 122103, India

<sup>8</sup> Department of Chemistry, Nitte Meenakshi Institute of Technology, Bengaluru, Karnataka 560064, India

<sup>9</sup> Research and Development Center, Department of Chemistry, Sir M. Visvesvaraya Institute of Technology (Affiliated to Visvesvaraya Technological University, Belagavi-590018), Bengaluru, Karnataka 562157, India

## 1 Introduction

NPs exhibit different chemical, physical, and biological properties compared to their bulk ones [1]. Among the transition metal oxides, ZnO is a versatile semi-conducting material. ZnO is an inorganic antimicrobial agent which is Generally Recognized As Safe (GRAS) under US-FDA listings, for human beings and animals [2–4]. It has unique properties like enormous binding energy, a wide band gap, and high thermal stability [5]. Due to its distinctive characteristics, ZnO is widely utilized in several industrial areas such as biosensors [6], transistors [6], magnetism [7], light emitting diodes [7], photocatalysts [8], textiles [9], leather industries [10], antimicrobial [8], and solar cells [11]. ZnO NPs have recently attracted a lot of attention in the discipline of cancer therapy [8]. ZnO NPs of various shapes, including spherical, pellet, polygonal, and rod have been prepared with varying particle sizes, and their cytotoxicity has been studied on murine, and cancer cells, including HepG-2, MCF-7, Colo320, HeLa, cloudman S91, tumour U87, MCF-7, HCT-116, A-549, PC-3, Calu-6, and DU-145 [8, 12–19]. ZnO NPs have been demonstrated in studies to produce cytotoxicity in a variety of cells, including human kidney cells, human hepatocytes, embryonic kidney cells, epithelial HT29 and Caco-2 cell lines, and glioma cells [20–22]. One of the primary applications of ZnO NPs is as an effective drug-delivery mechanism [23, 24]. Due to their distinct physical and chemical characteristics, ZnO NPs are one of the most utilised choices in DRUG delivery, cancer diagnostics, and treatment. It has been demonstrated that these NPs can target drugs in specific cells and tissues [23].

The biological synthesis of eco-friendly metallic NPs with well-defined sizes and forms is made possible by plants and their extracts. The enzyme, plant leaf extract, and bacteria play a vital role in synthesizing ZnO NPs [7]. Various approaches have been employed to synthesize ZnO nanocrystals such as solvothermal [25], sol-gel [26], direct precipitation [4], and hydrothermal [15]. Few of these methods require organic solvents, and reducing agents that may be toxic. These methods may have a longer experimental duration and pose potential environmental and biological risks with testing conditions. Solution Combustion Synthesis (SCS) is a fascinating process that involves the propagation of self-sustaining exothermic reactions in the presence of an aqueous medium. The advantages of SCS are that it is simple and convenient and the products can be obtained very quickly. The combustion approach is favored, because it ensures even distribution and atomic-level blending of the reactant with a combustible-fuel to produce of ultra-fine nanopowder [27–29].

*Piper betle* belongs to the Piperaceae family and is extensively grown in India, Srilanka, Thailand, Malaysia, Taiwan,

and other South Asian countries. It has been reported that Betle leaves have a broad spectrum of therapeutic properties. The extract of the *Piper betle* leaves possesses anti-mutagenic, anti-carcinogenic, anti-plaque, anti-diabetic, anti-inflammatory, antioxidant and antibacterial activities [30–33]. With the above background, herein we report the synthesis of ZnO NPs by SCS using an aqueous least extract of *Piper betle* as bio-fuel. Various techniques characterized the synthesized sample, and its anticancer activity was evaluated by MTT assay in MDA-MB-231 cell line. Further, its biocompatibility was examined by blood hemolysis.

## 2 Materials and methods

### 2.1 Chemicals

Zinc nitrate hexahydrate [ $\text{Zn}(\text{NO}_3)_2 \cdot 6\text{H}_2\text{O}$ ] (98% Sigma Aldrich) was used as precursor (oxidant). *Piper betel* leaves obtained from the plantations of Shimoga district (Karnataka, India) were used as fuel. Annexin V-FITC/PI (fluorescein isothiocyanate, propidium iodide) apoptosis detection kit was obtained from BD Bioscience, San Diego, California; 3-(4,5-dimethyl thiazol-2-yl)-2,5-diphenyl tetrazolium bromide (MTT), Dulbecco's Modified Eagle's Medium (DMEM) was purchased from Gibco and Crystal violet was bought from Himedia. All the chemicals used in this work were of analytical grade, without further purification.

## 3 Experimental

### 3.1 Plant extract preparation

The *Piper betel* leaves were washed with distilled water and air-dried. 50 g of leaves were ground with 10 mL of distilled water using a mechanical mixer at room temperature. The ground slurry of the leaves was added to 500 mL distilled water, boiled for 20 min, and then filtered through Whatman No. 1 filter paper. Filtrate was used to synthesize ZnO-PB-NPs.

### 3.2 Preparation of ZnO-PB-NPs

One gram of zinc nitrate was dissolved in 10 mL of double distilled water. 35 mL of the plant extract was added to the precursor. The mixture was stirred well using a magnetic stirrer for 10 min. The reaction mixture was taken in a crystallizing dish and placed in a preheated muffle furnace maintained at a temperature of  $430 \pm 10$  °C. The redox mixture, when heated, boiled, thermally dehydrated, and ignited to yield the voluminous product. The combustion product was

foamy, puffy, and porous. The schematic diagram of the synthesis of ZnO-PB-NPs is presented in Fig. 1.

### 3.3 Characterization

Various analytical techniques were adopted to characterize the ZnO-PB-NPs. The Powder X-ray Diffraction (PXRD) pattern was recorded using Panalytical X'pert Pro MPD powder X-ray diffractometer using Cu-K $\alpha$  radiation at  $\lambda = 1.5418 \text{ \AA}$ . FTIR spectrum was recorded (Nicolet Magna 50 FTIR spectrometer) in the wave number range 400–4000  $\text{cm}^{-1}$  with the KBr pellet technique. The morphology of the ZnO-PB-NPs was studied on SEM (SEM, VEGA3 TESCAN). TEM was employed to record the shape and particle size of ZnO-PB-NPs. Using the selected area electron diffraction (SAED) pattern from TEM (JOEL/JEM-2100), the phase developed was once again validated. To determine which components of the leaf extracts were responsible for combustion, phytochemical analyses were performed on the plant extract using established procedures [34–39].

### 3.4 Cell culture

The ATCC (American Type Culture Collection) provided the cell line of breast cancer (MDA-MB-231). The ATCC methodology was followed to culture, expand, and maintain the cells in DMEM media under conventional cell culture conditions like 100  $\mu\text{g}/\text{mL}$  streptomycin and 100 units/mL penicillin; supplemented with 10% fetal bovine

serum (calf serum) (Gibco BRL, Life Technologies, Grand-Island, NY, USA) under 5% carbon dioxide at 37 °C (Binder, Germany).

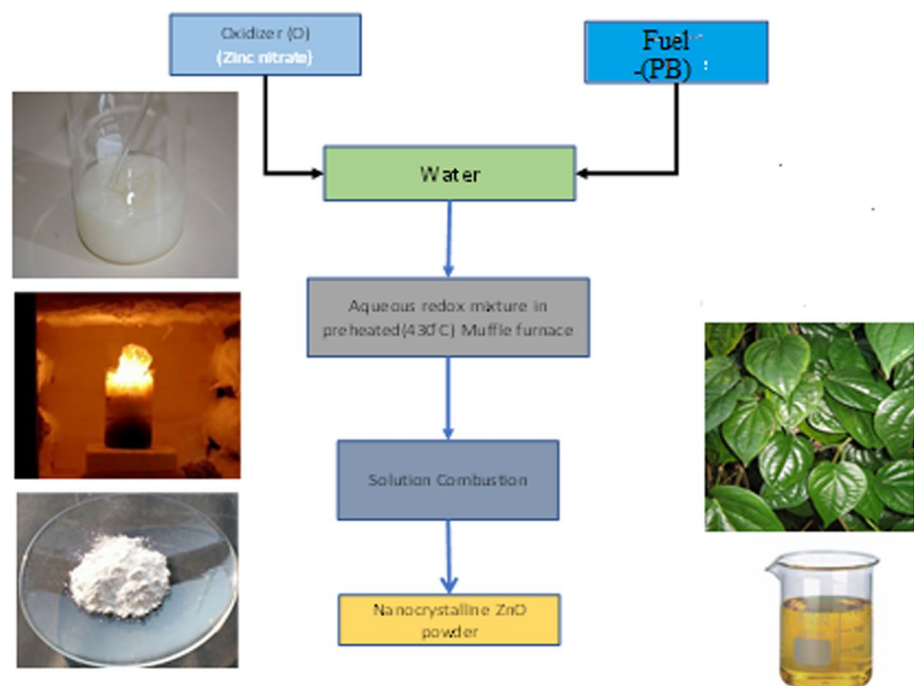
### 3.5 Cell growth inhibition assay

MDA-MB-231 cells were tested for the antiproliferative effect of ZnO-PB-NPs. At a density of  $5 \times 10^5$  cells/mL, the cancer cells were plated in a 96-well microplate. Different concentrations of ZnO-PB-NPs were used to treat each well and then incubated for further 24 h in a 5% CO<sub>2</sub> humidified environment at 37 °C. 20  $\mu\text{L}$  of MTT solution was then added to each well after the initial incubation, and the cells were then incubated again for additional 4 h at 37 °C in dark. In order to dissolve, water insoluble formazan crystals, 100  $\mu\text{L}$  of dimethyl sulfoxide (DMSO) was used. Using an ELISA (Tecan, Austria) reader, the cytotoxicity against cancer cells was assessed at 590 nm by measuring the absorbance. The negative control was the untreated medium with 0.1% vehicle DMSO. The percentage growth inhibition was calculated using the following formula:

$$\text{Percent inhibition} = \frac{(\text{OD of control} - \text{OD of sample}) \times 100}{\text{OD of control}}$$

The concentration of ZnO-PB-NPs required to inhibit the cell growth by 50% (IC<sub>50</sub>, the concentration at which cell growth is 50% inhibited) value was derived from the dose–response curve [40–44].

**Fig. 1** Schematic representation of synthetic route of ZnO-PB-NPs



### 3.6 Clonogenic survival assay

The clonogenic assay was performed as described in the literature with few modifications [45, 46]. MDA-MB-231 cells were seeded at  $3 \times 10^3$  cells into a six-well tissue culture plate and incubated in 5% CO<sub>2</sub> at 37 °C. After 24 h of incubation, the cells were treated with ZnO-PB-NPs of 10 µg/mL and 20 µg/mL. After 24 h of treatment, the medium was replaced with a complete growth medium, and cells were grown for 21 days to produce colonies with the intermittent medium replacement every 3 days. After 21 days, colonies were fixed with 4% paraformaldehyde in Phosphate Buffer Saline (PBS) for 30 min and then stained with 0.25% crystal violet. The dishes were rinsed with PBS and air-dried three times, and the number of colonies formed was visualized under an inverted microscope (Olympus). The colony is defined to consist of at least 50 cells.

$$\% \text{ of hemolysis} = \frac{(\text{Absorbance of control} - \text{Absorbance of sample})}{\text{Absorbance of control}} \times 100.$$

### 3.7 Annexin V-FITC/PI detection for cell apoptosis

ZnO-PB-NPs were applied to the MDA-MB-231 cells at a concentration of 10 µg/mL and 20 µg/mL for 24 h per well of  $1 \times 10^6$  cells. Control cells were untreated. Apoptosis was measured using the Annexin V-FITC/PI apoptosis detection kit (from BD Bioscience in San Diego, California). Following 15 min of dark incubation, the reaction was allowed to continue at room temperature with the addition of 5 µL of Annexin V-FITC and 5 µL of PI. The treated cells were then collected, washed twice with PBS, and suspended in the Annexin-V-binding solution. The cells were examined by flow cytometry using the Becton Drive fluorescence-activated cell sorting (BD FACS Calibre flow cytometer, United

States) in less than an hour. Cell Quest Pro software was used to analyse the data and find the apoptosis ratio [47].

### 3.8 Biocompatibility assay

Hemolysis assay was carried out as reported in the literature with certain modifications [48, 49]. About 5 mL of fresh human blood was obtained from a healthy volunteer and centrifuged at 1000 rpm for 10 min. The red blood cells (RBCs) were separated, washed twice with PBS, and diluted to a 1:4 ratio. PBS was used as a negative control, and 1% sodium dodecyl sulfate (SDS) was used as a positive control. Different concentrations of ZnO-PB-NPs were mixed with diluted erythrocytes suspension and incubated at 37 °C for 1 h. The tubes were centrifuged at 300 rpm for 5 min, the supernatant was collected, and absorbance was measured at 540 nm using a microplate reader (Tecan, Austria). The percentage of hemolysis was calculated as follows:

The samples were referred to be hemocompatible if the hemolysis rate is less than 5% and thus would be considered biocompatible [49].

## 4 Results and discussion

### 4.1 Qualitative phytochemical analysis of the aqueous leaf extracts of *Piper betle*

The results of qualitative phytochemical studies on *Piper betle* aqueous leaf extract are presented in Table 1. These findings support the presence of several phytochemicals

**Table 1** Results of phytochemical screening of aqueous leaf extract of *Piper betle*

Constituent	Test	Result	Constituent	Test	Result
Alkaloids	Mayer's reagent test	+	Tannins and Phenolic compounds	Lead acetate test	+
	Wagner's reagent test	+		Killer-Killiani test	-
	Hager's reagent test	+		Ferric chloride test	-
Carbohydrates	Molish's test	+	Saponins	Froth test	+
	Barfoed's test	+		Ninhydrin test	+
Reducing sugars	Fehling's test	+	Amino acids	Biuret test	+
	Benedict's test	-		Triterpenoids	Salwonski test
Flavanoids	Alkaline reagent test	+	and Steroids	Libermann and Burchard's test	-
	Lead acetate test	+		Carboxylic acids	Sodium bicarbonate test
Glycoside	Legal's test	+			Ester test
		Bomtrager's test	-		

+ is present, - is absent

**Fig. 2** Plausible mechanism of formation of ZnO-PB-NPs

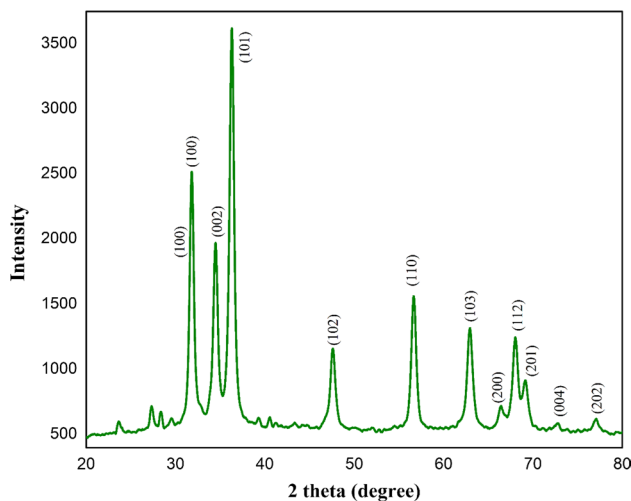
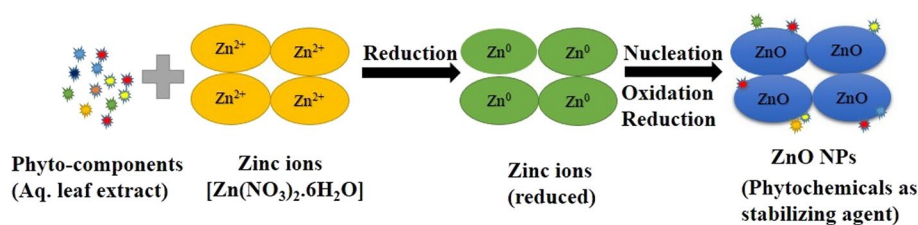


**Fig. 3** PXRD of ZnO-PB-NPs

in the aqueous extract of the leaves. The findings are nearly identical to those seen in the literature [50–52].

## 4.2 Mechanism of product formation

Plant leaf extracts contain phytochemicals that have an extraordinary ability to reduce metal ions in a much shorter time than fungus and bacteria, which require a longer incubation time [53]. As a result, plant leaf extracts are regarded as a good and safe source for the production of metal and metal oxide nanoparticles. Furthermore, plant leaf extract serves a dual purpose in the nanoparticle synthesis process by acting as both a reducing and a stabilizing agent. The compounds found in *Piper betel* leaf may be responsible for combustion. The following is the plausible mechanism for the development of ZnO-PB-NPs (Fig. 2).

## 4.3 Physico-chemical analysis

### 4.3.1 X-ray diffraction studies

The PXRD pattern shows that only a cubic phase was formed for the synthesized ZnO-PB-NPs as shown in Fig. 3. The ZnO-PB-NPs demonstrated crystallinity, with 2θ peaks located at 31.750°, (100); 34.440°, (002);

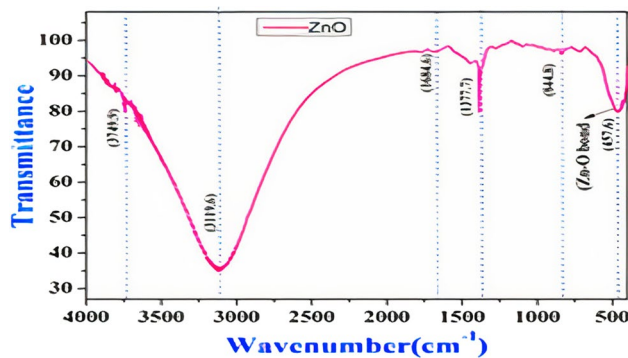


**Fig. 4** FTIR spectrum of ZnO-PB-NPs

36.252°, (101); 47.543°, (102); 56.555°, (110); 62.870°, (103); 66.388°, (200); 67.917°, (112); 69.057°, (201); 72.610°, (004); and 76.95°, (202). Moreover, the desired orientation (101) that corresponds to the plane was noticed. The peak at 2θ at 23.5° might be related to the orthorhombic Zn(OH)<sub>2</sub> phase [54]. This pattern is in accordance with the standard peaks displayed by the International Centre for Diffraction Data (ICDD card No. 80-0074). The indexation confirmed the standard hexagonal wurtzite structure. The obtained form is a hexagonal wurtzite structure. The wurtzite structure is most stable at ambient conditions and, thus, most common. Debye–Scherrer equation was followed to estimate the average crystallite size of the ZnO-PB-NPs, the formula expressed as  $D = \frac{0.94\lambda}{\beta \cos\theta}$ , where D = size of crystallite; 0.94 = shape factor; λ = 1.54 Å (CuKα radiation); β = FWHM (full width at half maxima) to (101) plane and θ = Bragg angle. The diameter of the crystallite was found to be 24 nm.

### 4.3.2 FTIR analysis

Utilizing FTIR spectrometer, the purity of the sample and the formation of ZnO bonding were confirmed. A typical FTIR spectrum of ZnO-PB-NPs is revealed in Fig. 4. The broad absorption peak at 3119.6 cm<sup>-1</sup> was attributable to the typical absorption of the hydroxyl group. The band



located at  $457.6\text{ cm}^{-1}$  was assigned to the stretch vibration of the Zn–O bond. These findings are in consistent with the reports available in the literature [18, 55].

### 4.3.3 Morphological studies and compositional analysis

**4.3.3.1 SEM studies** SEM was utilized to analyse the morphology of ZnO-PB-NPs. The surface morphology of ZnO-PB-NPs is depicted in Fig. 5a and b at various magnifications. The shape of the particles in the SEM micrograph was found to be spherical. The SEM scan could reveal that the majority of NPs were dispersed within a sizable matrix that resembles a frothy mass after the combustion process. The formation of ZnO-PB-NPs has an increased surface area and activity as a result of the numerous voids that were seen as a result of different gases escaping during the combustion phenomenon.

**4.3.3.2 EDAX analysis** The Energy Dispersive X-ray Analysis (EDAX) as shown in Fig. 6, reveals the ZnO-PB-NPs elemental composition and validates the zinc and oxygen signals of ZnO NPs. This investigation indicates that ZnO-PB-NPs were synthesised in their purest possible form; as evidenced by the elemental analysis, which revealed 69.97% zinc and 30.03% oxygen. The elemental analysis indicated that the ZnO sample formed was highly pure.

**4.3.3.3 TEM and SAED analysis** The surface morphology of ZnO-PB-NPs was affirmed through TEM. Figure 7a depicts the TEM of ZnO-PB-NPs. This image confirmed the spherical morphology of NPs. The ZnO-PB-NPs had particles in

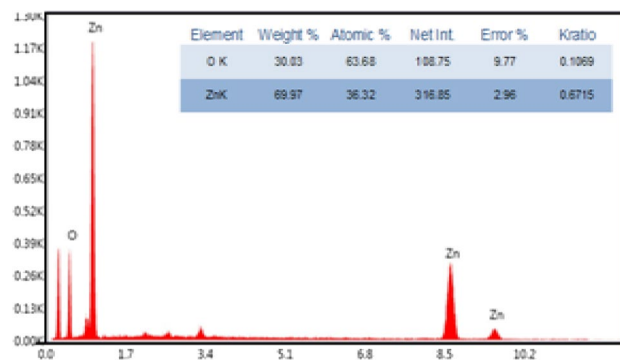


Fig. 6 EDAX image and elemental analysis of ZnO-PB-NPs

a diameter ranging between 25 and 35 nm. From Fig. 7a, it was evident that the sample had moderate particle aggregation which is consistent with the SEM results as shown in Fig. 4a and b.

From Fig. 7a, spacing of the lattice plane was determined to be 0.246 nm, which corresponds to the interspacing of the (101) plane of wurtzite ZnO. Figure 7b depicts the particles SAED pattern. The crystalline rings in SAED pattern could be indexed to the hexagonal wurtzite phase of ZnO.

## 4.4 Anti-cancer studies

### 4.4.1 ZnO-PB-NPs inhibited MDA-MB-231 cell proliferation

To investigate the effect of ZnO-PB-NPs on cancer cells, MTT assay was performed with their different concentrations (0, 0.3, 0.6, 1.25, 2.5, 5, 10, and 20  $\mu\text{g}/\text{mL}$ ) for 24 h.

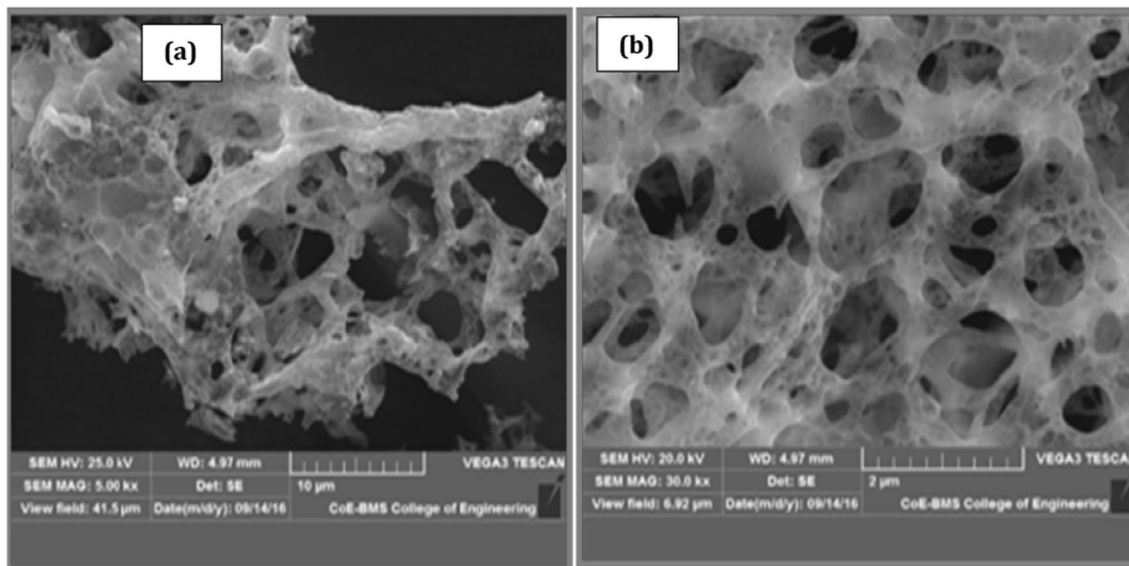
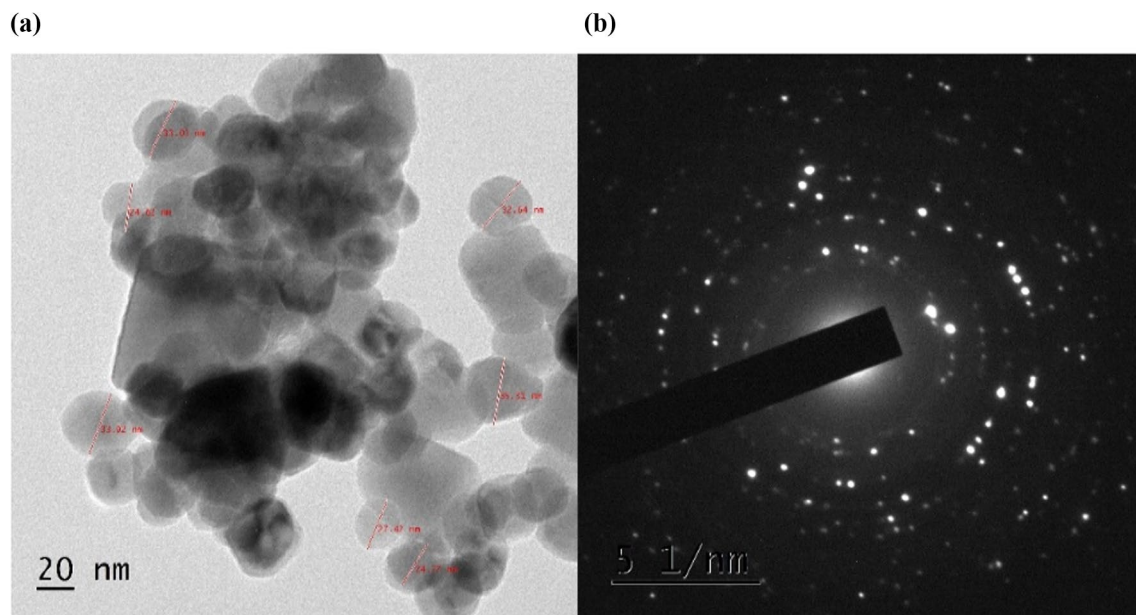
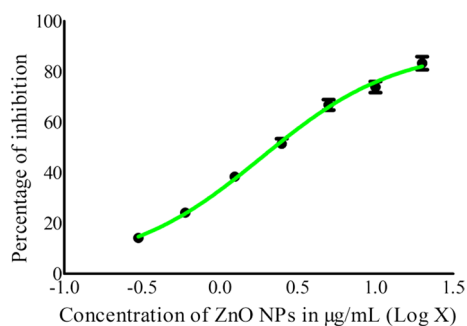


Fig. 5 a and b SEM Images of ZnO-PB-NPs at different magnifications



**Fig. 7** **a** TEM image and, **b** SAED pattern of ZnO-PB-NPs



**Fig. 8** IC<sub>50</sub> determination of ZnO-PB-NPs in MDA-MB-231 cells (Data represent  $\pm$  standard deviation)

It was observed that, upon ZnO-PB-NPs treatment, cell proliferation was inhibited in a concentration-dependent manner, and the maximum proliferation inhibition of 67% occurred at 20  $\mu\text{g/mL}$ . The IC<sub>50</sub> value of ZnO-PB-NPs on MDA-MB-231 was determined to be 1.89  $\mu\text{g/mL}$  by non-linear regression with Graphpad prism 5.0 (Graph Pad Software Inc., San Diego, USA) as presented in Fig. 8. These antiproliferative experiments show that ZnO-PB NP therapies sensitize cancer cells. Cell viability was found to diminish in a dose-dependent manner. The findings demonstrate that ZnO-PB-NPs achieved 67% cell viability at their highest concentration of 20  $\mu\text{g/mL}$  tested in our tests. According to the literature, ZnO-PB-NPs cause cytotoxicity in a cell-specific and proliferation-dependent way, with quiescent cells being the least

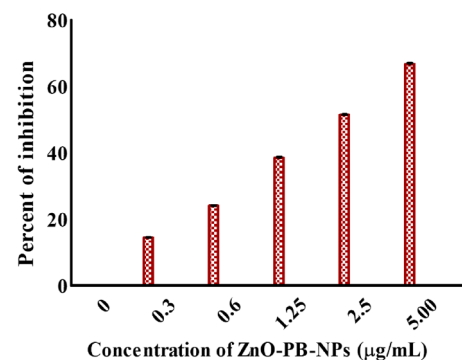
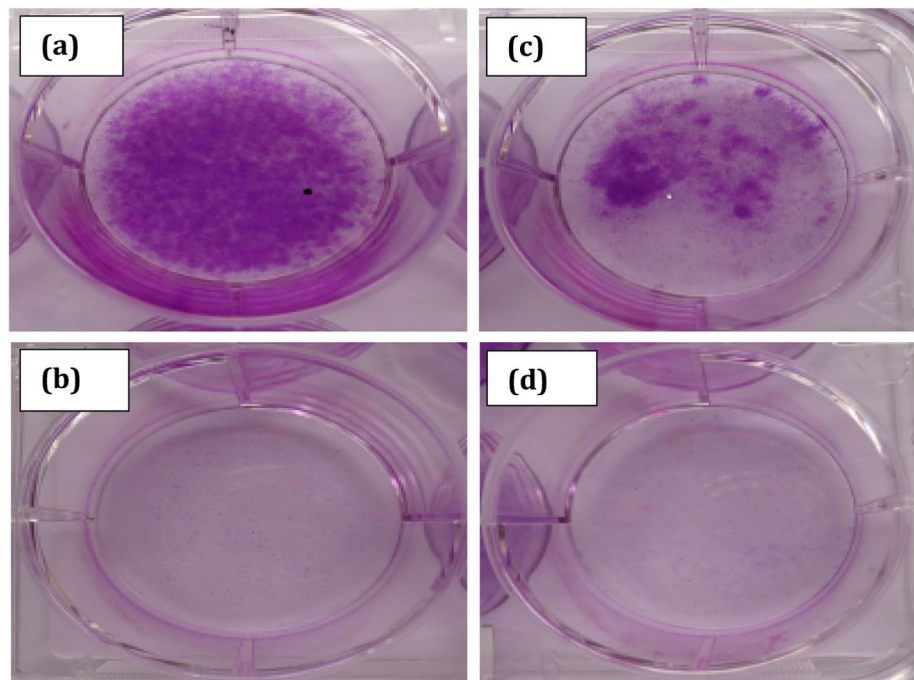


**Fig. 9** Cytotoxic effect of ZnO-PB-NPs on MDA-MB-231 cells. Cells were treated with various concentrations (0  $\mu\text{g/mL}$ , 0.3  $\mu\text{g/mL}$ , 0.6  $\mu\text{g/mL}$ , 1.25  $\mu\text{g/mL}$ , 2.5  $\mu\text{g/mL}$ , 5  $\mu\text{g/mL}$ ) of ZnO-PB-NPs. The percentage of cell death induced was determined using MTT assay

sensitive and rapidly dividing cancer cells being the most susceptible [56, 57].

Cytotoxic effect of ZnO-PB-NPs on MDA-MB-231 cells at various concentrations is presented in Fig. 9. Statistical analysis of the data was carried out by two-way ANOVA using Graphpad prism 5.0 (Graph Pad Software Inc., San Diego, USA). P-values 0.05 were assumed to be significant. ZnO-PB-NPs showed significant ( $p < 0.05$ ) cytotoxicity. The activity was found to be significant with 67% (average of three trials) inhibition at a concentration of 20  $\mu\text{g/mL}$ .

**Fig. 10** Clonogenic assay performed in 35 mm dish/six-well plate: **a** Untreated controlled cells, **b** Positive control Colchicine-20  $\mu$ M, **c** ZnO-PB-NPs-10  $\mu$ g/mL, and **d** ZnO-PB-NPs 20  $\mu$ g/mL



#### 4.4.2 Clonogenic assay

The Clonogenic assay has shown positive results in stopping the aggregations/agglomerations and growth of the cancer cell (MDA-MB-231). Clones were not seen in the 20  $\mu$ g/mL as in the case of the positive control Colchicine at 20  $\mu$ M [as shown in Fig. 10a–d].

#### 4.4.3 ZnO-PB-NPs-induced apoptosis in MDA-MB-231 cells

As it is well known, flow cytometry determines the amount of Deoxyribonucleic Acid (DNA) present in a cell based on its capacity to stain it most efficiently in a stoichiometric manner. Depending on the dye type, different locations on the DNA molecule are where these dyes bond. The blue-excited dye Propidium Iodide (PI) is the most widely used DNA-binding dye nowadays. Intercalating dye PI binds to double-stranded Ribonucleic Acid (RNA) and DNA. Restricted distribution of fluorescence intensities is found when diploid cells dyed with a dye that stoichiometrically binds to DNA are subjected to flow cytometric analysis. Apoptosis is clearly demonstrated by the translocation of phosphatidylserine molecules to the cell membrane's exterior due to phospholipid asymmetry. PI and Annexin V-FITC double staining were employed to establish the mechanism of cell death. The necrotic cells having membrane disruption allowed the dyes to link with the DNA. Still, early apoptotic cells excluded the DNA-binding dyes. ZnO-PB-NPs induced apoptosis on the MDA-MB-231 cell line was studied by the

MACSQuant analyzer and with the help of the MACSQuantify software [58, 59].

The flow cytometric analysis graphs showed the percentage of apoptosis and necrosis cells. LL1 stands for lower left quadrant cells (representing live cells) in the flow cytometric analysis histograms, LR1 for lower right quadrant early apoptotic cells, UR1 for upper right quadrant late apoptotic cells, and UL1 for upper left quadrant necrotic cells. The total apoptotic cell percentage was expressed by combining early and late apoptotic cells (LR1 and UR1 regions), the size and surface morphology, and the nanomaterial shape. The size of the NPs is also very important due to cause the particular biological status in terms of the cross the cell and its therapeutic values can be found out the biological tests through precise methods and materials and cure the cancerous cells and also no damage to the cell of any point and can cure the particular cancer cell lines are utilized for the test. Flow cytometry was used to encounter each cell, and what is the status of the cell and its shape and size. In MDA-MB-231 cells, ZnO-PB-NPs caused apoptosis. MDA-MB-231 cells underwent dose-dependent apoptotic induction by ZnO-PB-NPs. Following 10  $\mu$ g/mL for 48 h, apoptotic cells were 24.63% in MDA-MB-231 cells, and after 20  $\mu$ g/mL for 48 h, it was 35.01%, compared to 0% in untreated cells. The results showed that after ZnO-PB-NPs therapy, apoptosis was the main cause of cell death (Figs. 11, 12 and 13). These findings implied that there was a significant programmed cell death and hence ZnO-PB-NPs could be considered and subjected to further anticancer studies.



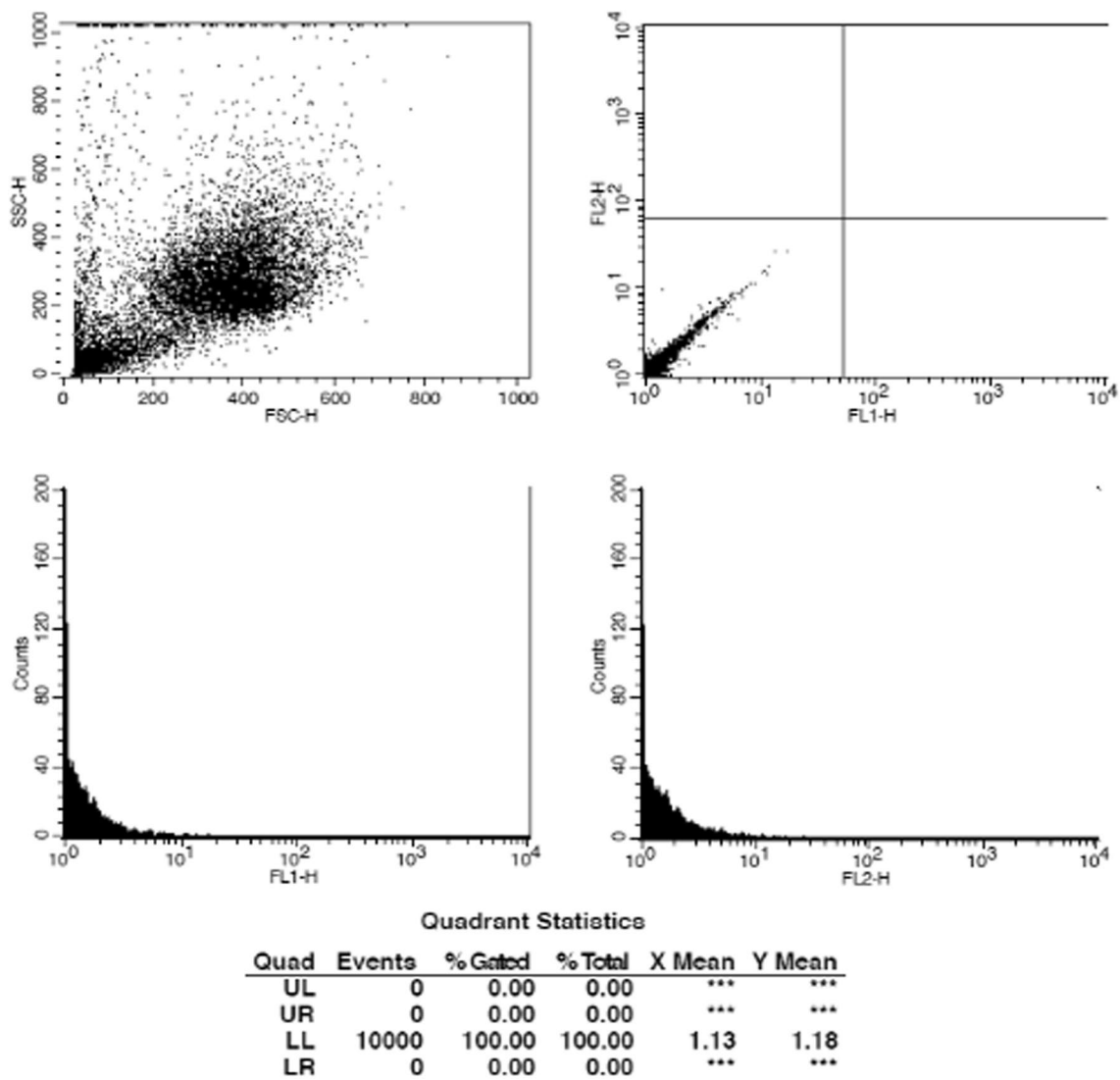


Fig. 11 Non-treated MDA-MB-231 cells

#### 4.4.4 Cell cycle studies

As analysed by flow cytometry, the effect of control, ZnO-PB-NPs and cochicine on the cell cycle in MDA-MB-231 cells is presented in Figs. 14, 15, 16 and 17. This data of cell cycle studies revealed how the test samples affected the cell cycle steps and it is given about the all, sub Go, Go/G1, S and G2M phases of the cell cycle by the left, Right events, % gated, % total, Mean and CV by columns wise of, Fig. 14; Cytometry plots of MDA-MB-231 cells treated with 1% DMSO as Control, Fig. 15; 10 µg/mL, Fig. 16; 20 µg/mL of ZnO-PB-NPs on MDA-MB-231 cancer cell lines and 20 µM of Colchicine extract along with the histogram statistics data [60].

The tables corresponding to Figs. 14, 15, 16 and 17 show the % gated, % total explained by all and the left and right, events and mean, and CV explains the histogram statistics of all phases of the cell at the different dosages of the ZnO-PB-NPs at 10 µg/mL, 20 µg/mL and the cytometry plot of MDA-MB-231 cells treated with 1% DMSO as control, flow cytometry plots of MDA-MB-231 NPs treated with 20 µM of Colchicine extract [61].

The ZnO-PB-NPs treatment at 10 µg/mL and 20 µg/mL has arrested 14.04% and 13.23% of MDA-MB-231 cells, respectively, at the G2M phase of the cell cycle, the increasing dose amount shows the saturation of concentration on further adding the sample of the concentration, therefore,

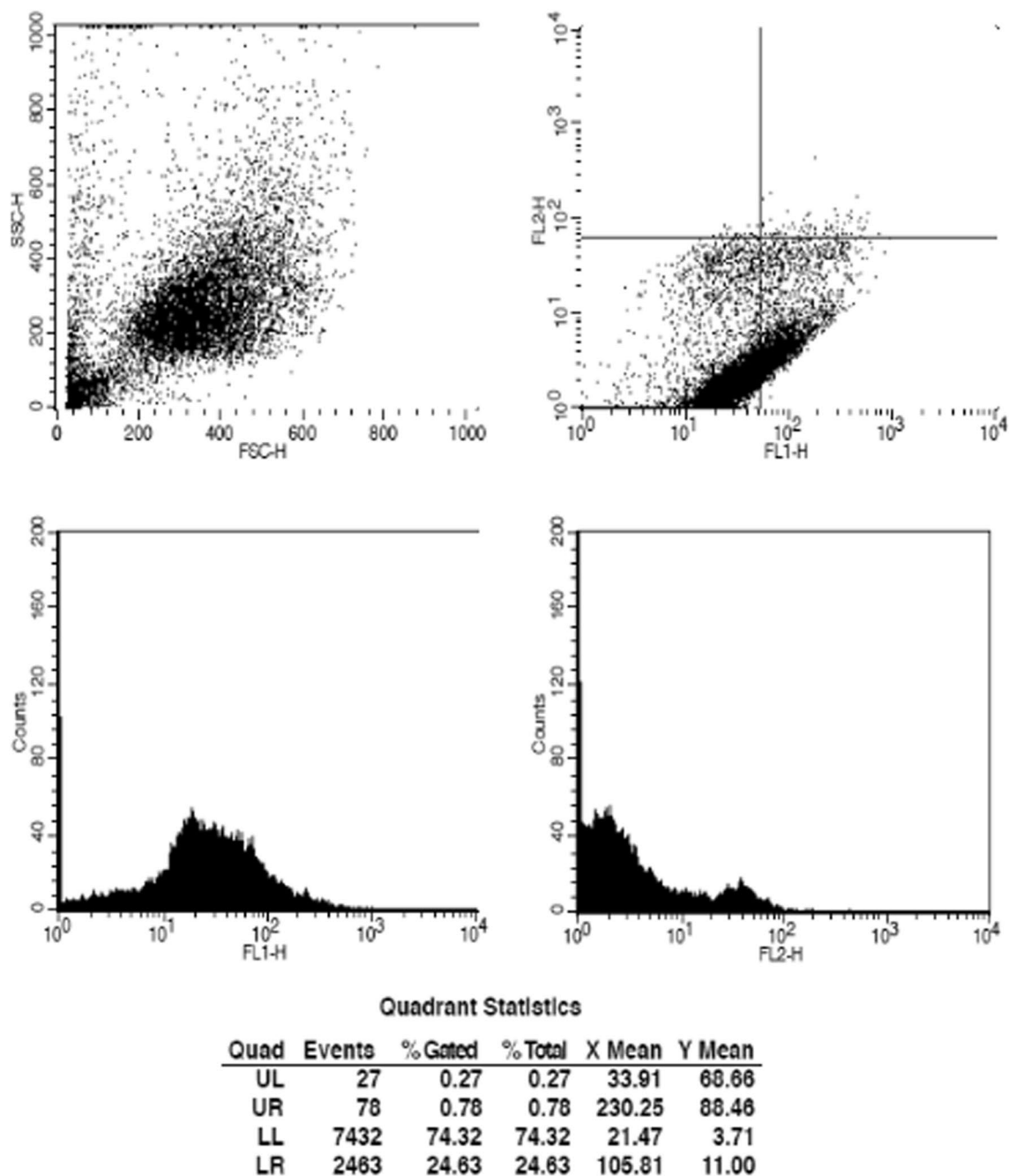


**Fig. 12** Treatment of MDA-MB-231 cells with 10 µg/mL of ZnO-PB-NPs

10 µg/mL is the ideal for the 14.04% arresting the MDA-MB-231 cancer cell line and damages the cell cycle path, similarly, compared to untreated MDA-MB-231 cells (6.25%). This result suggests that at both these concentrations of ZnO-PB-NPs, efficient cell cycle arrest at the G2M phase and a lower concentration of 10 µg/mL also seemed to be good.

#### 4.5 ZnO-PB-NPs are biocompatible

Biocompatibility testing is a prerequisite for applying ZnO-PB-NPs in a biological system. The hemolysis of erythrocytes in PBS, 1% SDS, and upon ZnO-PB-NPs treatment was examined by measuring their turbidity and lysis of erythrocytes at 540 nm. The hemolysis rate

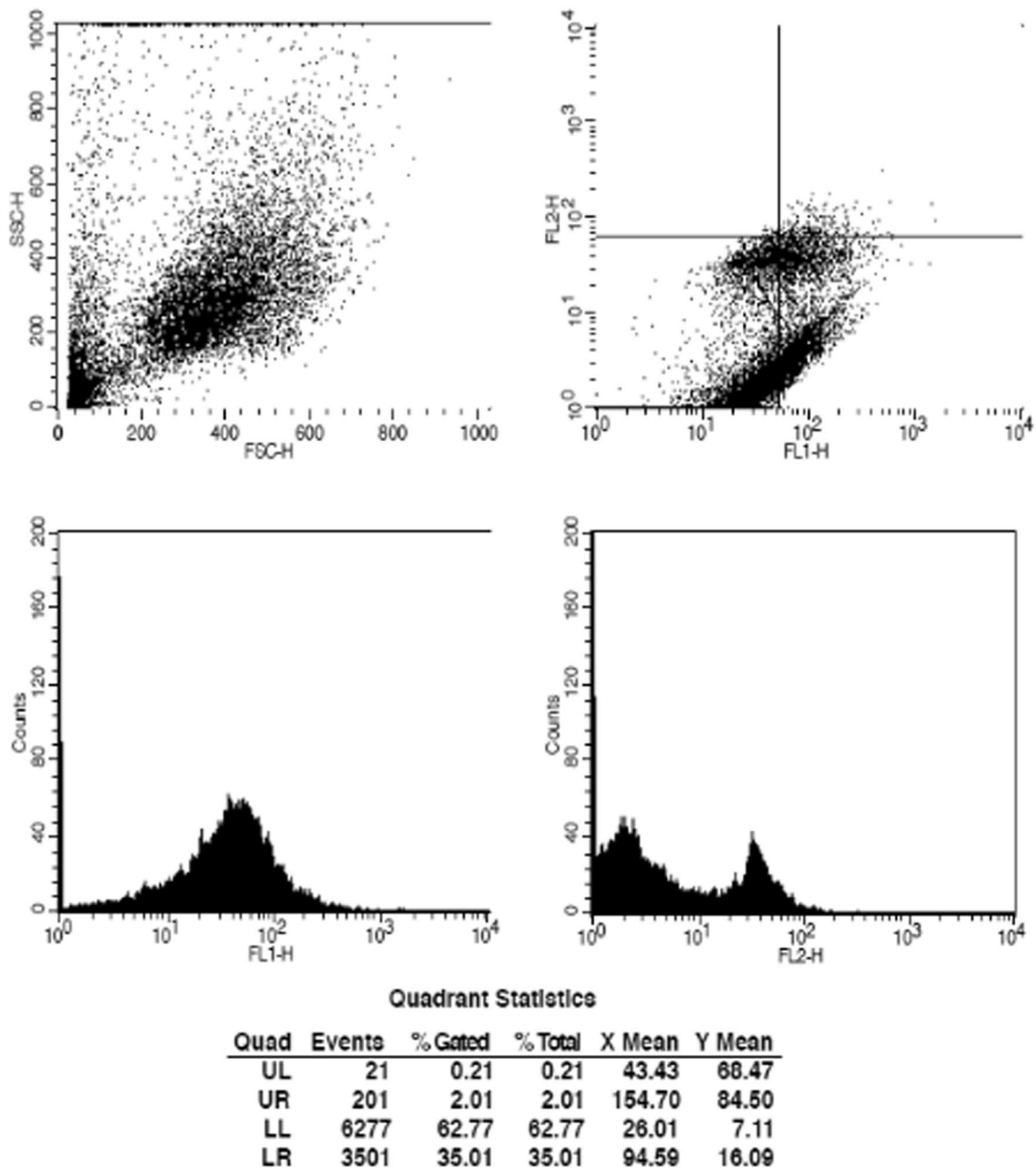


**Fig. 13** Treatment of MDA-MB-231 cells with 20  $\mu\text{g}/\text{mL}$  of ZnO-PB-NPs

at various concentrations of ZnO-PB-NPs treatment (10, 20, 40, 80, 160, and 320  $\mu\text{g}/\text{mL}$ ) showed significantly less hemolysis of 1.83, 3.05, 4.22, 6.29, 7.90, and 10.81%, respectively, compared to the negative control (2%) and positive control (100%). This study suggests that the ZnO-PB-NPs were biocompatible with no detectable hemolysis at the concentrations tested in our current studies for their anti-carcinogenic activity.

## 5 Conclusion

In conclusion, utilizing plant-assisted SCS, extremely porous ZnO-PB-NPs were produced. The sample was investigated extensively for its crystallinity, composition, and morphology. ZnO-PB-NPs exhibited anti-carcinogenic activity at very low concentrations. ZnO-PB-NPs treatment of MDA-MB-231 cells caused considerable dose-dependent

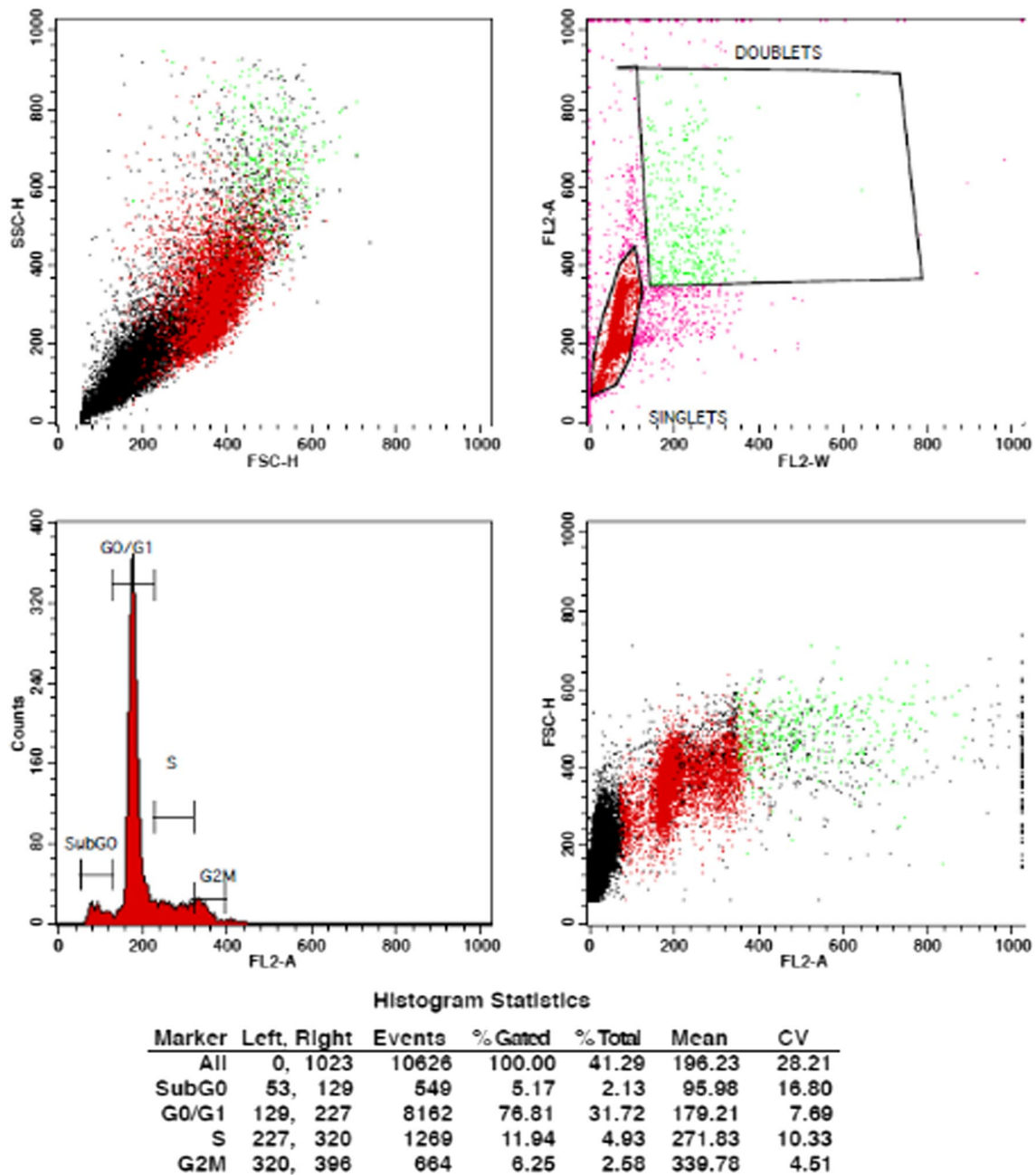
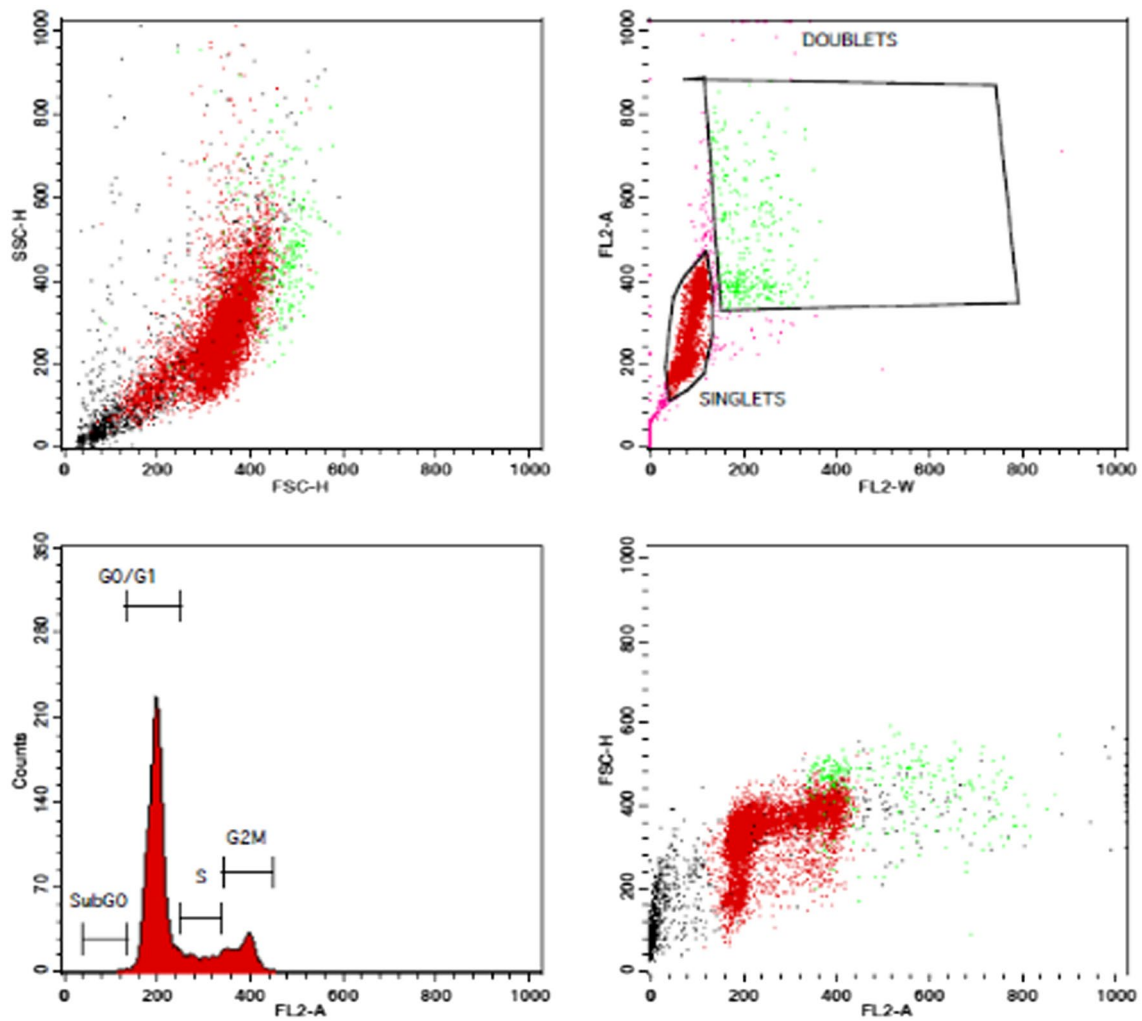


**Fig. 14** Cytometry and histogram statistics of MDA-MB-231 cells (treated with 1% DMSO as control)

cell death due to cytotoxicity. ZnO-PB-NPs boosted the generation of early apoptotic cell populations while decreasing breast cancer cell proliferation. ZnO-PB-NPs treatment impaired the clonogenic potential of breast cancer cells. The hemolytic assay revealed that ZnO-PB-NPs had an

insignificant effect on erythrocytes at low concentrations. This indicates the higher therapeutic potential of ZnO-PB-NPs. The findings of these studies will be significant for developing a potential anticancer therapeutic agent, a plausible alternative to conventional chemotherapy.





**Histogram Statistics**

Marker	Left	Right	Events	% Gated	% Total	Mean	CV
All	0	1023	10498	100.00	87.80	233.57	30.25
SubG0	41	133	18	0.17	0.15	125.39	4.83
G0/G1	133	249	7921	75.45	66.25	197.05	8.68
S	249	338	1025	9.76	8.57	292.35	9.29
G2M	344	449	1479	14.09	12.37	383.46	5.73

**Fig. 15** Flow cytometry plots of MDA-MB-231 cells treated with ZnO-PB-NPs (10 µg/mL), along with the histogram statistics

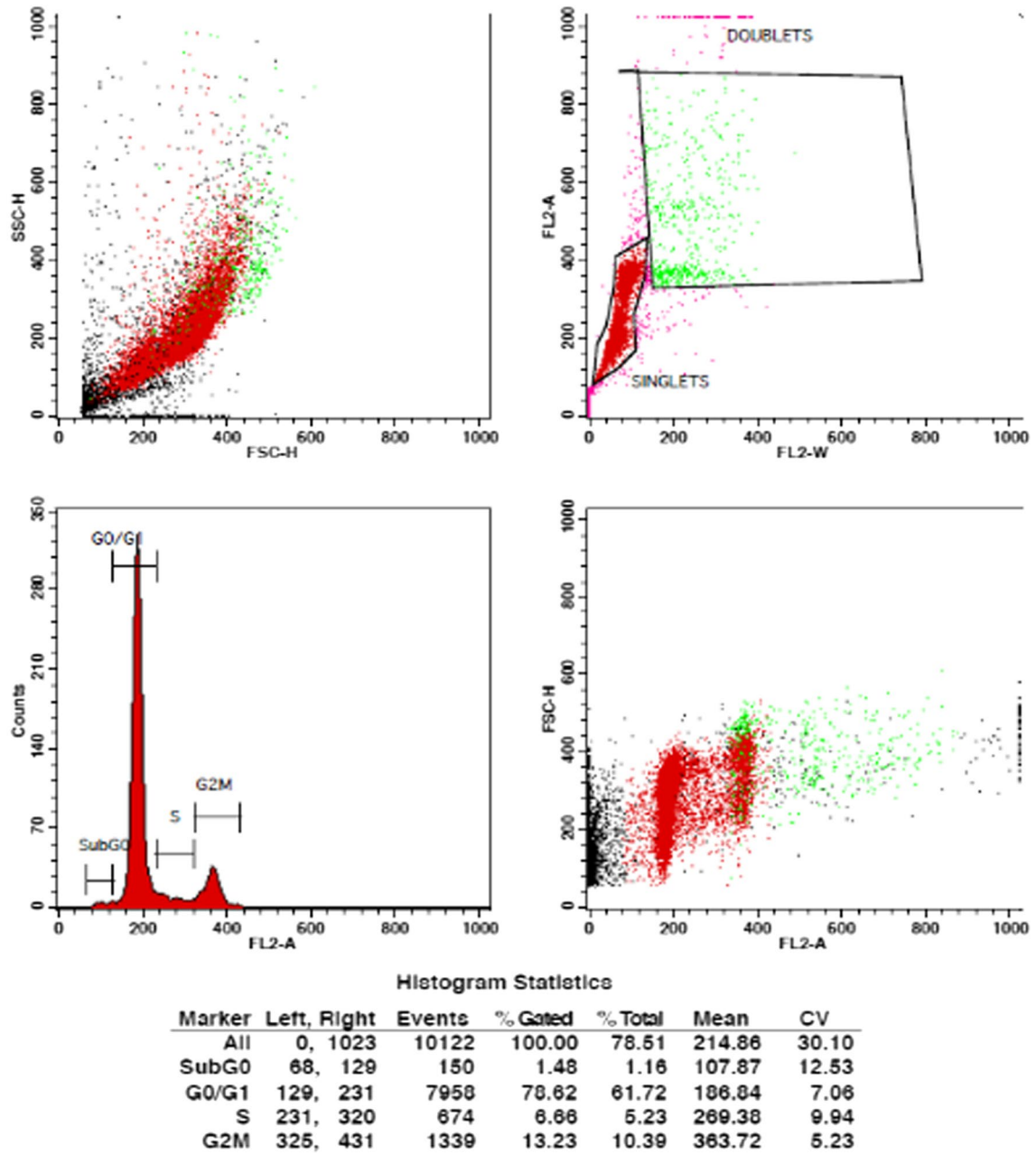


Fig. 16 Flow cytometry plots of MDA-MB-231 cells treated with ZnO-PB-NPs (20 µg/mL) along with the histogram statistics

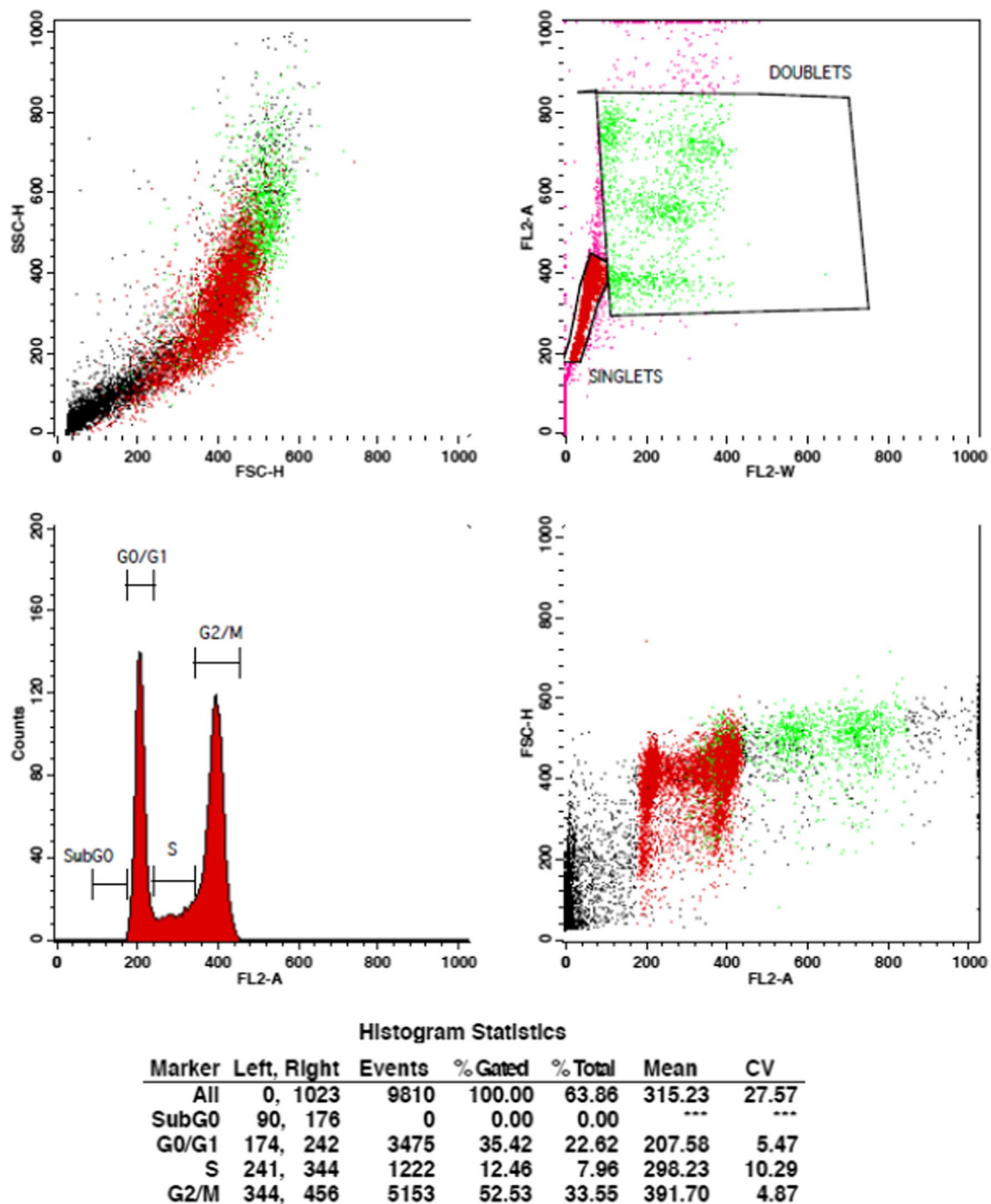


Fig. 17 Flow cytometry plots and histogram statistics of MDA-MB-231 cells following treatment with a 20 µM colchicine extract

**Acknowledgments** The author Dr. Shobha Nagarajaiah is thankful to Dr. Shivashankarappa L.H., Principal, Maharani’s Science College for Women, Bengaluru for the support. Dr. Prashanth GK would like to express his gratitude to the management of Sri KET for the constant encouragement provided towards research activities.

**Author contributions** Conceptualization, generation of the hypothesis, experimentation, and manuscript writing SN, PGK and NN; software

analysis, SN, PGK, NN, PM, MGG, and SR; review and editing PGK, SN, and NN; revision plagiarism errors and proofread, PGK, SN, NN, PM, BMN, MG, and SR. All authors have read and agreed to the published version of the manuscript.

**Data availability** Not applicable.

## References

1. S. Wang, K. Cheng, K. Chen, C. Xu, P. Ma, G. Dang et al., Nanoparticle-based medicines in clinical cancer therapy. *Nano Today* **45**, 101512 (2022). <https://doi.org/10.1016/j.nantod.2022.101512>
2. H. Mohd Yusof, R. Mohamad, U.H. Zaidan et al., Microbial synthesis of zinc oxide nanoparticles and their potential application as an antimicrobial agent and a feed supplement in animal industry: a review. *J Anim Sci Biotechnol* **10**, 57 (2019). <https://doi.org/10.1186/s40104-019-0368-z>
3. M.C. Sportelli, C. Gaudiuso, A. Volpe, M. Izzì, R.A. Picca, A. Ancona, N. Cioffi, Biogenic synthesis of ZnO nanoparticles and their application as bioactive agents: a critical overview. *Reactions* **3**, 423–441 (2022). <https://doi.org/10.3390/reactions3030030>
4. P.G. Krishna, P.P. Ananthaswamy, T. Yadavalli, N.B. Mutta, A. Sannaiah, Y. Shivanna, ZnO nanopellets have selective anticancer activity. *Mater. Sci. Eng. C* **62**, 919–926 (2016). <https://doi.org/10.1016/j.msec.2016.02.039>
5. I. Shahine, N. Beydoun, J.J. Gaumet, E.-E. Bendeif, H. Rinnert, P. Magri, A. EnNaciri, P. Miska, S. Jradi, S. Akil, Pure, size tunable ZnO nanocrystals assembled into large area PMMA layer as efficient catalyst. *Catalysts* **9**, 162 (2019). <https://doi.org/10.3390/catal9020162>
6. R.A. Salinas, A. Orduña-Díaz, O. Obregon-Hinostroza, M.A. Dominguez, Biosensors based on zinc oxide thin-film transistors using recyclable plastic substrates as an alternative for real-time pathogen detection. *Talanta* **237**, 122970 (2022). <https://doi.org/10.1016/j.talanta.2021.122970>
7. H.-Q. Liu, C.-B. Yao, Y. Cai, H.-T. Yin, Synthesis, photoluminescence and photocatalytic characteristics of Ag–ZnO sandwich structures. *J.Phys. Chem. Solids* **165**, 110697 (2022). <https://doi.org/10.1016/j.jpcs.2022.110697>
8. P.G. Krishna, P. Chandra Mishra, M.M. Naika, M. Gadewar, P.P. Ananthaswamy, S. Rao, S.R. Boselin Prabhu, K.V. Yatish, H.G. Nagendra, M. Moustafa et al., Photocatalytic activity induced by metal nanoparticles synthesized by sustainable approaches: a comprehensive review. *Front. Chem.* **10**, 917831 (2022). <https://doi.org/10.3389/fchem.2022.917831>
9. J. Xu, Y. Huang, S. Zhu, N. Abbes, X. Jing, L. Zhang, A review of the green synthesis of ZnO nanoparticles using plant extracts and their prospects for application in antibacterial textiles. *J. Eng. Fibers Fabr.* **16**, 15589250211046242 (2021). <https://doi.org/10.1177/15589250211046242>
10. J. Liu, J. Ma, Y. Bao, J. Wang, H. Tang, L. Zhang, Polyacrylate/surface-modified ZnO nanocomposite as film-forming agent for leather finishing. *Int. J. Polym. Mater. Polym. Biomater.* **63**, 809–814 (2014). <https://doi.org/10.1080/00914037.2014.886217>
11. M. Manabeng, B.S. Mwankemwa, R.O. Ocaya, T.E. Motaung, T.D. Malevu, A review of the impact of zinc oxide nanostructure morphology on perovskite solar cell performance. *Processes* **2022**, 10 (1803). <https://doi.org/10.3390/pr10091803>
12. P.G. Krishna, P.P. Ananthaswamy, M. Gadewar, U. Bora, N.B. Mutta, In vitro antibacterial and anticancer studies of ZnO nanoparticles prepared by sugar fueled combustion. *Synthesis* **8**, 24–29 (2017). <https://doi.org/10.5185/amLett.2017.6424>
13. P.G. Krishna, P.P. Ananthaswamy, N.B. Mutta, K.G. Mariyappa, R. Singh, Comparison of antimicrobial and anticancer activity of ZnO nanoparticles prepared using different precursors by hydrothermal synthesis. *J. Chem. Pharm. Sci.* **10**, 192–197 (2017)
14. G.K. Prashanth, P.A. Prashanth, P. Singh, B.M. Nagabhushana, C. Shivakumara, G.M. Krishnaiah et al., Effect of doping (with cobalt or nickel) and UV exposure on the antibacterial, anticancer, and ROS generation activities of zinc oxide nanoparticles. *J. Asian Ceram. Soc.* **8**(4), 1175–1187 (2020). <https://doi.org/10.1080/21870764.2020.1824328>
15. G.K. Prashanth, P.A. Prashanth, B.M. Nagabhushana, S. Ananda, H.G. Nagendra, R.C. Singh, In vitro antimicrobial, antioxidant and anticancer studies of ZnO nanoparticles synthesized by precipitation method. *Adv. Sci. Eng. Med.* **8**, 306–313 (2016). <https://doi.org/10.1166/asem.2016.1854>
16. G.K. Prashanth, P.A. Prashanth, M. Ramani, S. Ananda, B.M. Nagabhushana, G.M. Krishnaiah et al., Comparison of antimicrobial, antioxidant and anticancer activities of ZnO nanoparticles prepared by lemon juice and citric acid fueled solution combustion synthesis. *BioNanoScience* **9**(4), 799–812 (2019). <https://doi.org/10.1007/s12668-019-00670-8>
17. L. Palanikumar, S. Ramasamy, C. Balachandran, Antibacterial and cytotoxic response of nano zinc oxide in gram negative bacteria and colo 320 human adenocarcinoma cancer cells. *Curr. Nanosci.* **9**, 469–478 (2013). <https://doi.org/10.2174/1573413711309040009>
18. F. Namvar, H.S. Rahman, R. Mohamad, S. Azizi, P.M. Tahir, M.S. Chartrand, S.K. Yeap, Cytotoxic effects of biosynthesized zinc oxide nanoparticles on murine cell lines, *Evid. Based Complement. Alternat. Med.* **2015**, 593014 (2015). <https://doi.org/10.1155/2015/593014>
19. R. Wahab, M.A. Siddiqui, Q. Saquib, S. Dwivedi, J. Ahmad, J. Musarrat, A.A. AlKhedhairi, H.-S. Shin, ZnO nanoparticles induced oxidative stress and apoptosis in HepG2 and MCF-7 cancer cells and their antibacterial activity. *Colloids Surf. B: Biointerfaces* **117**, 267–276 (2014). <https://doi.org/10.1016/j.colsurfb.2014.02.038>
20. I. Pujalte, I. Passagne, B. Brouillaud, M. Treguer, E. Durand, C. Ohayon-Courtes, B. L'Azou, Cytotoxicity and oxidative stress induced by different metallic nanoparticles on human kidney cells. *Part. Fibre Toxicol.* **8**, 10 (2011). <https://doi.org/10.1186/1743-8977-8-10>
21. R. Guan, T. Kang, F. Lu, Z. Zhang, H. Shen, M. Liu, Cytotoxicity, oxidative stress, and genotoxicity in human hepatocyte and embryonic kidney cells exposed to ZnO nanoparticles. *Nanoscale Res. Lett.* **7**, 602 (2012). <https://doi.org/10.1186/1556-276X-7-602>
22. T. Kang, R. Guan, X. Chen, Y. Song, H. Jiang, J. Zhao, In vitro toxicity of different-sized ZnO nanoparticles in Caco-2 cells. *Nanoscale Res. Lett.* **8**, 496 (2013). <https://doi.org/10.1186/1556-276X-8-496>
23. E. Taylor, T.J. Webster, Reducing infections through nanotechnology and nanoparticles. *Int. J. Nanomed.* **6**, 1463–1473 (2011). <https://doi.org/10.2147/IJN.S22021>
24. H. Mirzaei, M. Darroudi, Zinc oxide nanoparticles: biological synthesis and biomedical applications. *Ceram. Int.* **43**(1, Part B), 907–914 (2017). <https://doi.org/10.1016/j.ceramint.2016.10.051>
25. Y. Hu, L. Sun, Z. Liu, T. Liu, Controlled solvothermal synthesis of ZnO nanoparticles using non-destructive Mg-based channel templates for enhanced photocatalytic performance. *Mater. Chem. Phys.* **299** (2023). <https://doi.org/10.1016/j.matchemphys.2023.127525>
26. M. Lal, P. Sharma, L. Singh, C. Ram, Photocatalytic degradation of hazardous Rhodamine B dye using sol-gel mediated ultrasonic hydrothermal synthesized of ZnO nanoparticles. *Results Eng.* **17**, 100890 (2023). <https://doi.org/10.1016/j.rineng.2023.100890>
27. K.C. Patil, S.C. Aruna, T. Mimani, Combustion synthesis: an update. *Curr. Opin. Solid State Mater. Sci.* **6**(6), 507–512 (2002). [https://doi.org/10.1016/S1359-0286\(02\)00123-7](https://doi.org/10.1016/S1359-0286(02)00123-7)



28. K.C. Patil, M.S. Hegde, R. Tanu et al., *Chemistry of Nanocrystalline Oxide Materials* (World Scientific, Singapore, 2008). [https://doi.org/10.1016/S1359-0286\(02\)00123-7](https://doi.org/10.1016/S1359-0286(02)00123-7)
29. N. Shobha, N. Nanda, A.S. Giresha, P. Manjappa, S. P, K.K. Dharmappa et al., Synthesis and characterization of Zinc oxide nanoparticles utilizing seed source of *Ricinus communis* and study of its antioxidant, antifungal and anticancer activity. *Mater. Sci. Eng.: C* **97**, 842–850 (2019). <https://doi.org/10.1016/j.msec.2018.12.023>
30. T. Nalina, Z.H.A. Rahim, The crude aqueous extract of *Piper betle* L. and its antibacterial effect towards *Streptococcus mutans*. *Am. J. Biotechnol. Biochem.* **13**, 10–15 (2007). <https://doi.org/10.3844/ajbbsp.2007.10.15>
31. L.S.R. Arambewela, L.D.A.M. Arawwawala, W.D. Ratnasooriya, Antidiabetic activities of aqueous and ethanolic extracts of *Piper betle* leaves in rats. *J. Ethnopharmacol.* **13**, 239–245 (2005). <https://doi.org/10.1016/j.jep.2005.06.016>
32. R. Hajare, V.M. Darvhekar, A. Shewale, V. Patil, Evaluation of antihistaminic activity of piper betel leaf in guinea pig. *Afr. J. Pharm. Pharmacol.* **13**, 113–117 (2011)
33. N. Nur-Sazwi, T. Nalina, Z.H.A. Rahim, Antioxidant and cytoprotective activities of *Piper betle*, *Areca catechu*, *Uncaria gambir* and betel quid with and without calcium hydroxide. *BMC Complement. Altern. Med.* **13**, 351 (2013). <https://doi.org/10.1186/1472-6882-13-351>
34. C.K. Kokate, *Practical Pharmacognosy* (Vallabh Prakashan, New Delhi, 2000)
35. J.B. Harbone, *Phytochemical Methods* (Chapman and Hall, London, 1999)
36. P. Tiwari, B. Kumar, M. Kaur et al., Phytochemical screening and extraction: a review. *Internationale Pharmaceutica Scientia.* **1**, 98–106 (2011)
37. G.K. Prashanth, G.M. Krishnaiah, Chemical composition of the leaves of *Azadiracta indica* Linn (Neem). *Int. J. Adv. Eng. Technol. Manag. Appl. Sci.* **1**(5), 21–31 (2014)
38. G.K. Prashanth, G.M. Krishnaiah, H.M. Sathyananda, Qualitative phytochemical screening and GCMS analysis of the leaves of *Indigofera tinctoria*. *Int. J. Innov. Res. Sci. Eng. Technol.* **4**, 7544–7547 (2015). <https://doi.org/10.15680/IJRSET.2015.0408080>
39. G.K. Prashanth, G.M. Krishnaiah, Phytochemical screening and GC-MS analysis of the leaves of *Pongamia Pinnata* linn. *Int. J. Innovative Res. Sci. Eng. Technol.* **3**(11), 17329–17334 (2014). <https://doi.org/10.15680/IJRSET.2014.0311034>
40. T. Mosmann, Rapid colorimetric assay for cellular growth and survival: application to proliferation and cytotoxicity assays. *J. Immunol. Methods* **65**, 55–63 (1983). [https://doi.org/10.1016/0022-1759\(83\)90303-4](https://doi.org/10.1016/0022-1759(83)90303-4)
41. G.K. Prashanth, H.M. Sathyananda, P.A. Prashanth, M. Gadevar, M. Mutthuraju, S.R. Boselin Prabhu et al., Controlled synthesis of Ag/CuO nanocomposites: evaluation of their antimycobacterial, antioxidant, and anticancer activities. *Appl. Phys. A* **128**, 614 (2022). <https://doi.org/10.1007/s00339-022-05748-x>
42. H.M. Sathyananda, P.A. Prashanth, G.K. Prashanth, B.M. Nagabhushana, C. Shivakumara, S.R. Boselin Prabhu et al., Evaluation of antimycobacterial, antioxidant, and anticancer activities of CuO nanoparticles through cobalt. Doping. *Appl. Nanosci.* (2021). <https://doi.org/10.1007/s13204-021-02156-0>
43. H.M. Sathyananda, P.A. Prashanth, G.K. Prashanth, B.M. Nagabhushana, G.M. Krishnaiah, H.G. Nagendra, Antimicrobial, antioxidant, and cytotoxicity activities of CuO nanopellets synthesized by surfactant-free hydrothermal method. *J. Test. Evaluat.* (2021). <https://doi.org/10.1520/JTE20200538>
44. P. Gopala Krishna, P. Paduvarahalli Ananthaswamy, P. Trivedi, V. Chaturvedi, N. Bhangi Mutta, A. Sannaiah et al., Antitubercular activity of ZnO nanoparticles prepared by solution combustion synthesis using lemon juice as bio-fuel. *Mater. Sci. Eng. C* **75**, 1026–1033 (2017). <https://doi.org/10.1016/j.msec.2017.02.09>
45. N.A.P. Franken, H.M. Rodermond, J. Stap, J. Haveman, C. van Bree, Clonogenic assay of cells in vitro. *Nat. Protoc.* **1**(5), 2315–2319 (2006). <https://doi.org/10.1038/nprot.2006.339>
46. J.S. K oerich, D.J. Nogueira, V.P. Vaz, C. Simioni, M.L.N.D. Silva, L.C. Ouriques, D.S. Vicentini, W.G. Matias, Toxicity of binary mixtures of Al<sub>2</sub>O<sub>3</sub> and ZnO nanoparticles toward fibroblast and bronchial epithelium cells. *J. Toxicol. Environ. Health A* **83**(9), 363–377 (2020). <https://doi.org/10.1080/15287394.2020.1761496>
47. K. Rjiba-Touati, I. Ayed-Boussema, H. Hamdi, S. Abid, Genotoxic damage and apoptosis in rat glioma (F98) cell line following exposure to bromuconazole. *Neurotoxicology* **94**, 108–116 (2023). <https://doi.org/10.1016/j.neuro.2022.11.006>
48. M.C. Pico, A. Basulto, A. del Monte, A. Hidalgo, M.E. Lanio, C. Alvarez et al., Cross-reactivity and inhibition of haemolysis by polyclonal antibodies raised against St II, a cytolysin from the sea anemone *Stichodactyla helianthus*. *Toxicon* **43**, 167–171 (2004). <https://doi.org/10.1016/j.toxicon.2003.11.020>
49. D. Das, B.C. Nath, P. Phukon, S.K. Dolui, Colloid. Surf. B: Bio Interfaces. **101**, 430–433 (2013)
50. S. Biswal, Phytochemical analysis and a study on the antiestrogenic antifertility effect of leaves of Piper betel in female albino rat. *Anc. Sci. Life.* **34**(1), 16–22 (2014). <https://doi.org/10.4103/0257-7941.150770>
51. R. Rajamani, K. Selvam, S. Muthusamy, R. Devadass, Preliminary phytochemical screening of aqueous extract of betel nut and betel leaves. *Int. J. Biosci. Nanosci.* **3**(1), 14–18 (2026)
52. N.M. Patel, D.D. Jain, H.P. Suryawanshi, S.P. Pawar, Phytopharmacological study of *Piper Betle* leaf, Saudi. *J. Med. Pharm. Sci.* (2019). <https://doi.org/10.36348/sjmps.2019.v05i11.008>
53. A.K. Jha, K. Prasad, V. Kumar, K. Prasad, Biosynthesis of silver nanoparticles using eclipta leaf. *Biotechnol. Prog.* **25**, 1476–1479 (2009). <https://doi.org/10.1002/btpr.233>
54. S. Wongrerkrdee, S. Wongrerkrdee, C. Boonruang, S. Sujinnapram, Enhanced photocatalytic degradation of methylene blue using Ti-doped ZnO nanoparticles synthesized by rapid combustion. *Toxics* **11**, 33 (2023). <https://doi.org/10.3390/toxics11010033>
55. K. Handore, S. Bhavsar, A. Horne, P. Chhattise, K. Mohite, J. Ambekar, N. Pande, V. Chabukswar, Novel green route of synthesis of ZnO nanoparticles by using natural biodegradable polymer and its application as a catalyst for oxidation of aldehydes. *J. Macromol. Sci. Part A* **51**(12), 941–947 (2014). <https://doi.org/10.1080/10601325.2014.967078>
56. R.J. Gonzalez, J.B. Tarloff, Evaluation of hepatic subcellular fractions for Alamar blue and MTT reductase activity. *Toxicol. In Vitro* **15**, 257–259 (2001). [https://doi.org/10.1016/S0887-2333\(01\)00014-5](https://doi.org/10.1016/S0887-2333(01)00014-5)
57. L. Kangas, M. Gr nroos, A.L. Nieminen, Bioluminescence of cellular ATP: a new method for evaluating cytotoxic agents in vitro. *Med. Biol.* **62**, 338–343 (1984)
58. F. Blankenberg, J. Narula, H.W. Strauss, In vivo detection of apoptotic cell death: a necessary measurement for evaluating therapy for myocarditis, ischemia, and heart failure. *J. Nucl. Cardiol.* **6**, 531–539 (1999). [https://doi.org/10.1016/S1071-3581\(99\)90026-0](https://doi.org/10.1016/S1071-3581(99)90026-0)
59. M.A. Swairjo, N.O. Concha, M.A. Kaetzel, J.R. Dedman, B.A. Seaton, Ca<sup>2+</sup>-bridging mechanism and phospholipid head group recognition in the membrane-binding protein annexin V. *Nat. Struct. Biol.* **2**, 968–974 (1995). <https://doi.org/10.1038/nsb1195-968>

60. J. Zhang, L. Tan, C. Wu, Y. Li, H. Chen, Y. Liu et al., Discovery and biological evaluation of 4,6-pyrimidine analogues with potential anticancer agents as novel colchicine binding site inhibitors. *Eur. J. Med. Chem.* **248**, 115085 (2023). <https://doi.org/10.1016/j.ejmech.2022.115085>
61. I.K. Lindamulage, H.-Y. Vu, C. Karthikeyan, J. Knockleby, Y.-F. Lee, P. Trivedi et al., Novel quinolone chalcones targeting colchicine-binding pocket kill multidrug-resistant cancer cells by inhibiting tubulin activity and MRP1 function. *Sci. Rep.* **7**, 10298 (2017). <https://doi.org/10.1038/s41598-017-10972-0>

**Publisher's Note** Springer Nature remains neutral with regard to jurisdictional claims in published maps and institutional affiliations.

Springer Nature or its licensor (e.g. a society or other partner) holds exclusive rights to this article under a publishing agreement with the author(s) or other rightsholder(s); author self-archiving of the accepted manuscript version of this article is solely governed by the terms of such publishing agreement and applicable law.